Printable ink holograms

Zhao, Qiancheng; Yetisen, Ali K.; Anthony, Carl J.; Fowler, William R.; Yun, Seok Hyun; Butt, Haider

DOI:
10.1063/1.4928046

AIP Applied Physics Letters

Printable ink holograms

Qiancheng Zhao, Ali K. Yetisen, Carl J. Anthony, William R. Fowler, Seok Hyun Yun, and Haider Butt

Citation: Applied Physics Letters **107**, 041115 (2015); doi: 10.1063/1.4928046
View online: http://dx.doi.org/10.1063/1.4928046
View Table of Contents: http://scitation.aip.org/content/aip/journal/apl/107/4?ver=pdfcov
Published by the AIP Publishing

Printable ink holograms

Qiancheng Zhao,[1,a)] Ali K. Yetisen,[2,a)] Carl J. Anthony,[1] William R. Fowler,[1] Seok Hyun Yun,[2] and Haider Butt[1,b)]
[1]*Nanotechnology Laboratory, School of Mechanical Engineering, University of Birmingham, Edgbaston, Birmingham B15 2TT, United Kingdom*
[2]*Harvard Medical School and Wellman Center for Photomedicine, Massachusetts General Hospital, 50 Blossom Street, Boston, Massachusetts 02114, USA*

(Received 21 May 2015; accepted 24 July 2015; published online 29 July 2015)

The development of single-step printable holographic recording techniques can enable applications in rapid data storage, imaging, and bio-sensing. The personalized use of holography is limited due to specialist level of knowledge, time consuming recording techniques, and high-cost equipment. Here, we report a rapid and feasible in-line reflection recording strategy for printing surface holograms consisting of ink using a single pulse of a laser light within seconds. The laser interference pattern and periodicity of surface grating as a function of tilt angle are predicted by computationally and demonstrated experimentally to create 2D linear gratings and three-dimensional (3D) images. We further demonstrate the utility of our approach in creating personalized handwritten signatures and 3D images. © *2015 AIP Publishing LLC*. [http://dx.doi.org/10.1063/1.4928046]

Holograms have been the focus of enormous research in recent years. They offer a remarkable level of spatial resolution and multiplexing capability that is not achievable with any other image recording techniques. Their exploitation holds potential in optical applications such as three-dimensional (3D) displays, smart windows, security, optical interferometers, and biosensors.[1–3] An off-axis hologram is typically recorded by projecting an interference pattern consisting of scattered light from an object with a coherent reference wave. The recorded image can be replayed using a mono/polychromatic light source to reconstruct the wavefront by means of diffraction.[4–6] The historical recording of permanent images in photosensitive media is based on multi-beam interference and wet chemistry involving silver halides or photoresists to create volumetric or surface gratings.[7–11] In the case of surface gratings, the master hologram may be copied through embossing by surface stamping.[12–15] In surface holograms recorded in photoresist, the main limitation is the high cost involved in preparing the master hologram, which limits the utilization of holography for personalized applications. In silver-halide volume holograms, the image needs to be copied using laser light, followed by development and fixing steps. Alternatively, photopolymers (Polaroid DMP-128) maybe utilized to record holograms. However, this method requires an additional step of exposure to regular light of uniform intensity to stabilize the hologram. Furthermore, wet processing is required to control the colour and bandwidth of the hologram. Holograms can also be recorded by complex methods such as E-beam lithography (EBL)[16] and focussed ion beam (FIB) milling,[17] which are still low-throughput, labour-intensive, and costly. To overcome these limitations, direct laser interference patterning (DLIP) in split-beam off-axis mode has been utilized to ablate surface gratings. Laser pulses (275–300 mJ/cm^2) were utilized to ablate a range of materials including polymers, aluminium zinc oxide, nickel, and steel.[18–20] This ablation setup can be integrated with an optical head with variable spatial period from 0.40 to 3.75 μm at a working distance of 35 mm. In another approach, a frequency-quadrupled diode-pumped solid-state laser (6 ns, 266 nm, 20 mJ) allowed direct interference ablation of light-emitting fluorene polymer ADS133YE to create gratings that were 5 mm in diameter.[21] Ti:sapphire laser with regenerative amplification (130 fs, 800 nm) was also utilized to create surface gratings in polymethyl methacrylate (PMMA).[22] In these approaches, the laser pulse was split into two beams that are focused by two identical lenses and then symmetrically aligned to be incident on the sample. This approach also known as off-axis interference requires accurate interferometric alignment of laser beams and limits the use of 3D objects in laser ablation mode due to the significant decrease in the intensity of laser light after beam splitting. Hence, the ability to print 2D gratings and/or 3D images with the use of a single laser pulse in an optically flexible mode using low-cost materials for rapid production to achieve personalized holograms remains a challenge.

Here, we show a rapid, single-pulse laser ablation strategy to print 2D and 3D surface holograms within seconds. We first computationally design the recording of surface gratings for in-line "Denisyuk" reflection holography in ablation mode. The diffraction characteristics of surface gratings are evaluated computationally for various diffraction angles as the grating hologram is illuminated with violet, green, and red light. We then fabricate holograms by using a high-energy nanosecond pulsed laser. We analyze the post-ablation effects through characterizing their optical properties by topographical imaging and angular-resolved measurements using reflection spectrophotometry. Finally, we further demonstrate the applications of our laser ablation methodology by showing 2D surface and 3D coin holograms. Laser ablation can be employed to produce various surface holograms based on a variety of complex surfaces and photo-absorption materials, offering the potential for the production of optical devices.

[a)]Q. Zhao and A. K. Yetisen contributed equally to this work.
[b)]Author to whom correspondence should be addressed. Electronic mail: h.butt@bham.ac.uk.

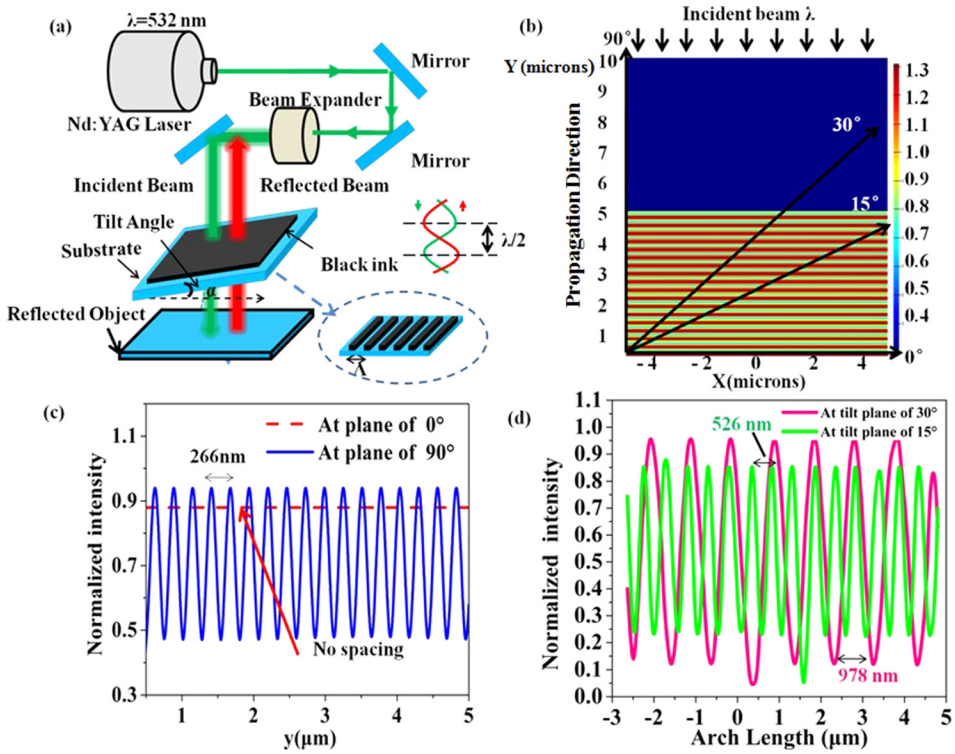

FIG. 1. Laser ablation holography in Denisyuk "reflection" mode. (a) Schematic of laser setup for recording surface ink holograms. (b) 2D intensity distribution image of single laser beam interference. (c) Simulated optical intensity profile plots at plane of 0° and 90°, respectively. (d) Simulated plots of interfering intensity profile at tilt planes of 15° and 30°, respectively.

The surface holograms were recorded based on "Denisyuk" reflection interference in ablation mode (Figure 1(a)). 150 nm thick ink (Lumocolor, Staedtler) was deposited on a PMMA substrate by spin coating at 2100 rpm for 3 s. A Nd-yttrium-aluminum-garnet pulsed laser with a second-harmonic generator (5 ns, 350 mJ @ 532 nm, 10 Hz, thermally stabilized with wavelength separation) was used to print the surface gratings in Denisyuk reflection mode. The ink was patterned through a single 5 ns (~10 mJ) laser pulse (10 Hz, Q-switch delay = 400 μs) directed toward the recording media tilted (α) from the horizontal plane. In a single 5 ns exposure, the ablated spot area was 1 cm^2. We utilized a single pulse strategy to record the holograms. Producing a grating over an area of 1 cm^2 required 5 ns. To create images of larger samples, multiple laser exposures were required to cover 5 cm^2 by manually moving a XY translation stage. Therefore, using a laser operating at 10 Hz, ablated regions were not limited by the laser pulse, but the speed of the XY translation stage. The use of robotic XY translation stages can increase the ablation area. A reflecting object (i.e., mirror) was placed normal to the laser incidence beam under the recording medium. The reflected beam and the incident beam travelling in opposite directions interfered and created a standing wave, which created a periodic constructive interference. The ink was then ablated at a periodicity related to the incident wavelength of the laser beam

$$y = y_1 + y_2 = A\cos 2\pi\left(\nu t - \frac{x}{\lambda}\right) + A\cos 2\pi\left(\nu t + \frac{x}{\lambda}\right) = \left|2A\cos 2\pi\frac{x}{\lambda}\right|\cos 2\pi\nu t, \quad (1)$$

where y_1 and y_2 represents the incident (reference) and reflected (object) laser beam propagations, respectively. The standing wave oscillates in time but has spatial dependence (propagation direction) which is stationary, and the constructive interfering peak occurs at intervals of approximately $\lambda/2$. However, as the substrate is tilted from horizontal, the periodicity can be controlled by the tilt angle. We simulated the 2D intensity distribution of the standing wave as a function of tilt angle by finite difference time domain (FDTD) method.

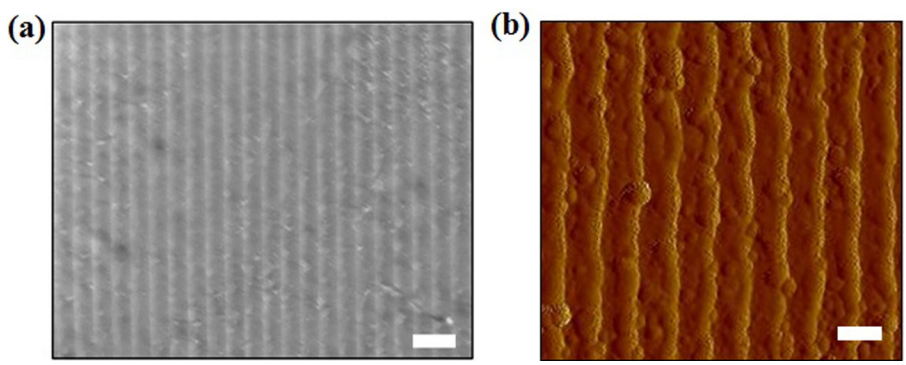

FIG. 2. Images of recorded linear surface gratings. (a) Environmental scanning electron microscope image of the surface grating. Scale bar = 5 μm. (b) AFM characterization showing thickness and spacing of surface ink-grating. Scale bar = 3 μm.

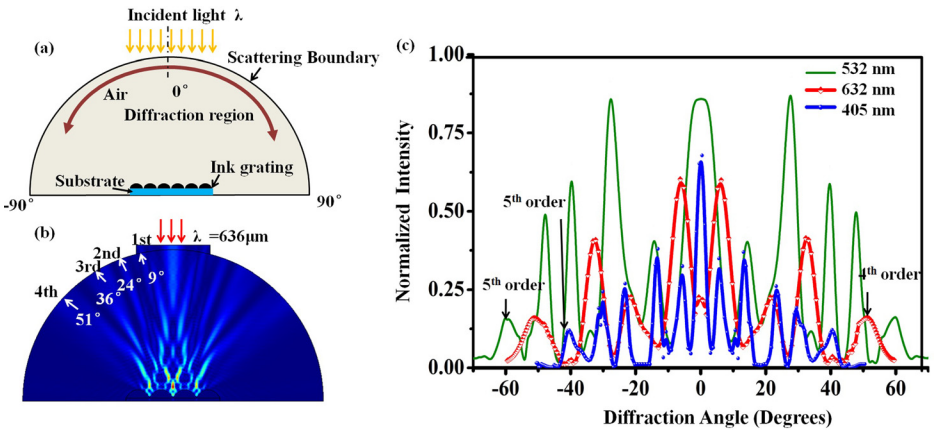

FIG. 3. Diffraction model of the surface gratings. (a) Sketch of simulation geometry for ink-based grating. (b) Far-field diffraction pattern by shining red laser (636 nm) on the grating. (c) Diffraction intensity profile plots across the hemispherical boundary as a function of angle in response to three incident wavelengths.

Figure 1(b) shows the interference intensity distribution by a laser beam ($\lambda = 532$ nm), the resultant intensity alternated from peak to valley uniformly, indicating well-ordered grating pattern. Figure 1(c) illustrates the intensity profile across the planes of 0°and 90°. There was uniform spacing of ~266 nm ($\lambda/2$) at 90° while no varying optical intensity was observed at plane of 0°, and thus no fringes will be formed when the sample is ablated normal to the incident beam. Optical intensity distribution in other tilt planes was also simulated as shown in Figure 1(d). The value of periodicity is

$$\Lambda = \frac{\lambda}{2\sin\alpha}, \tag{2}$$

where α is the tilt angle of sample from the surface plane, and λ is the incident wavelength. By changing the tilt angle, the spacing of holographic grating can be controlled. The gratings periods were 3052, 1532, 1028, and 777 nm at tilt angles of 5°, 10°, 15°, and 20°, respectively.

Figure 2(a) shows an environmental electron scanning microscope (ESEM) image of the fabricated gratings with a periodicity of ~2.6 μm, which is in agreement with Eq. (2).

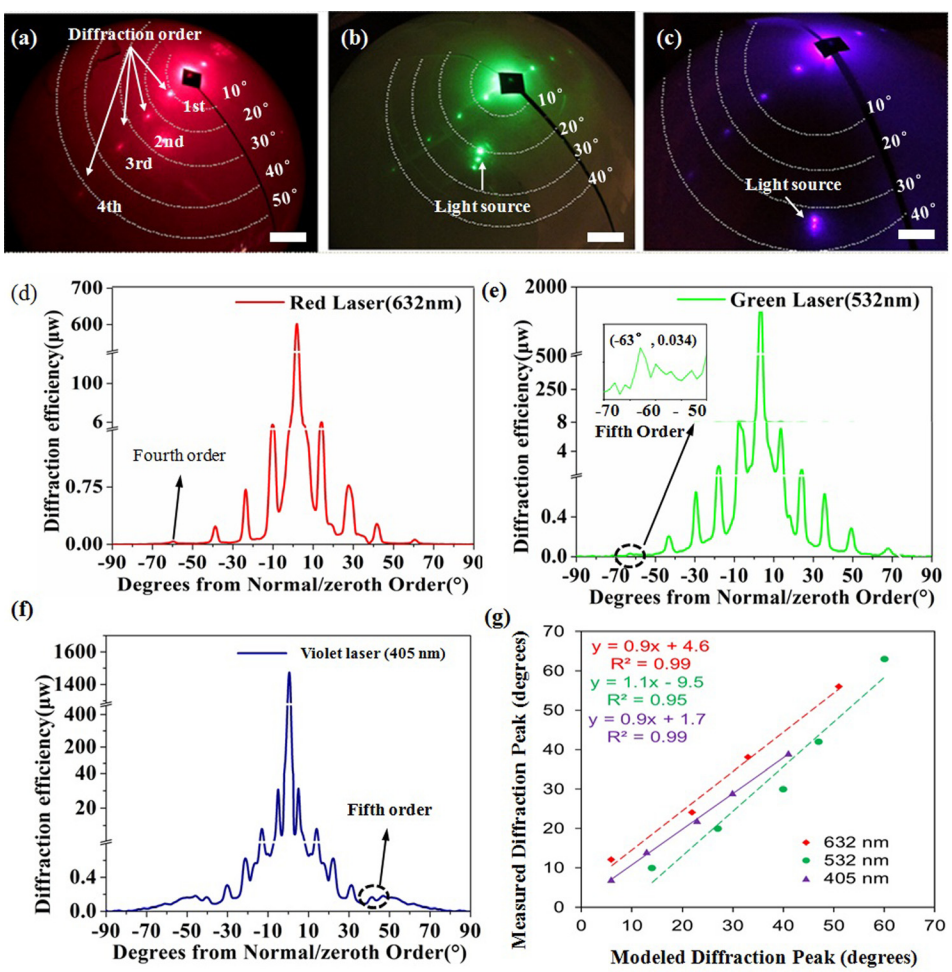

FIG. 4. Optical characterization of the surface gratings by angular-resolved measurements. Diffraction patterns obtained on the screen of the integrating-sphere by shining (a) red ($\lambda = 632$ nm), (b) green ($\lambda = 532$ nm), and (c) violet ($\lambda = 405$ nm) light sources directed perpendicularly to the surface grating. Scale bar = 5 mm. Diffraction spectra as a function of rotation degree at (d) red ($\lambda = 636$ nm), (e) green ($\lambda = 532$ nm), and (f) violet light ($\lambda = 405$ nm). (g) Correlation between the angles of the simulated and experimental diffraction peaks.

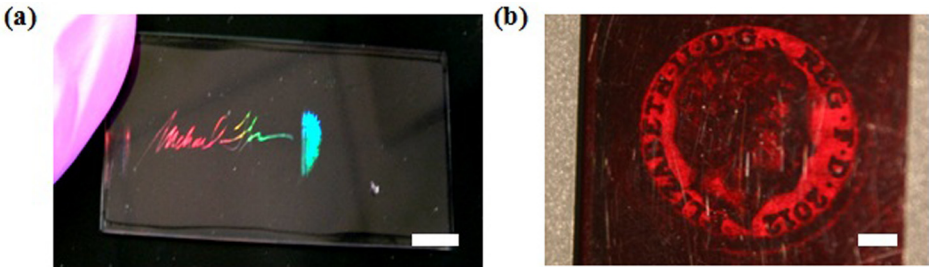

FIG. 5. Surface holograms recorded by single nanosecond laser interference. (a) Ink-based holographic signature. (b) 3D holographic coin. Scale bars = 5 mm.

The periodicity of the grating was further supported by AFM characterization showing ~150 nm average depth of ink layer (Fig. 2(b)).

The diffraction pattern of the ablated grating was simulated by means of finite element method (FEM) using COMSOL Multiphysics, a Ø32 μm hemispherical boundary was modeled to show diffraction pattern by far-field projection. Three different wavelengths (405, 532, and 632 nm) were induced to illuminate the ink-based grating at a normal incidence. The dimensions of grating were modeled according to the ESEM and AFM data. The 2D geometry model for grating is shown in Figure 3(a).

Figure 3(b) shows the diffraction pattern in response to red light, and four symmetrical diffraction orders were observed. Figure 3(c) illustrates the simulated angular-resolved spectra for 632, 532, and 405 nm light. Five diffraction orders were visualized by violet and green light, and the diffraction angles increased as the incident light was shifted to longer wavelength for the same order. The simulated diffraction spectra showed that the grating had four orders under red light (6°, 22°, 33°, and 51°), five orders under green light (14°, 27°, 40°, 47°, and 60°), and five orders under violet light (6°, 13°, 23°, 30°, and 41°).

The diffraction spectra of ink surface hologram were measured using a semitransparent integrating sphere setup. The sample was illuminated vertically by red, green, and violet monochromatic light sources and diffraction spots were projected on the screen of the hemisphere as shown in Figures 4(a)–4(c).

Multiple diffraction orders were observed corresponding to each incident wavelength; this was due to the large spacing which distributed the incident light energy into different diffraction orders. In addition, the diffraction spots situated symmetrically from the center of hemisphere, with violet diffracted at lower angle and red at higher angle, which is in agreement with the simulated model.

To assess the diffraction angles and efficiency as a function of wavelength, angular-resolved measurements were conducted. The structure for holding sample and light source was supported by a stepping motor, which was capable of rotating from −90° to 90° of the normal/zeroth order with 1° increments. An optical power meter was placed in front of the 3D rotational stage to capture the diffraction spots.

Figures 4(d)–4(f) display the diffraction intensity for the three wavelengths as a function of rotation angle. A symmetrical number of peaks were observed on each side of the non-diffracted zeroth order although there was less than 1 μW distinction (<0.1%) in peak intensity between each sides. The diffraction spectra showed that the grating had four orders under red light (12°, 24°, 38°, and 56°), five orders under green light (10°, 20°, 30°, 42°, and 63°), and five orders under violet light (7°, 14°, 22°, 29°, and 39°). Figure 4(g) shows the correlation between angles of the measured and simulated diffraction peaks. The presented model allowed predicting the diffraction angles with R^2 values of 0.99, 0.95, and 0.99 for red, green, and violet light, respectively. The decrease in the prediction ability for the green-violet light region may be attributed to absorption of light by the ink in this region. A weak diffraction intensity for fifth order was captured at green and violet lasers incidence. The experimental diffraction efficiencies were calculated by adding all scattered spots in transmissive and reflective directions. For example, in the sample illuminated by 405 nm wavelength, the total diffraction efficiency was 8.43% by adding ten (five spots from each side of normal) transmissive spots in forward direction and ten reflective spots in backward direction. For the diffraction efficiency, ~55% and ~45% contributed to transmissive and reflective diffractions, respectively.

We demonstrate the application of nanosecond laser ablation by presenting a holographic 2D signature and a 3D coin image. Figure 5(a) shows a handwritten signature hologram. The signature was handwritten on a PMMA substrate and then patterned by laser ablation. In recording holograms greater than 1 cm^2, multiple exposures were required to ablate the sample surface in different areas using a XY linear translation stage to cover the signed region. The diffracted image was polychromatic when illuminated with a white light source. This holographic signature may be applied to personalizing and authenticating certain kinds of autograph. Figures 5(b) illustrates a 3D coin hologram, which was fabricated by the setup provided in Figure 1(a). However, in this case, the object was replaced by a coin to enable the information of coin to be recorded. The diffracted image showed 3D vision disparity from different perspectives; however, monochromatic virtual coin images could be reconstructed when illuminated with a laser beam.

In conclusion, we developed a technique to print surface gratings using single laser ablation holography in Denisyuk reflection mode. The grating spacing that would be written into the printable ink was predicted by computational simulation at tilt angles of 15°, 30°, and 90°. The periodicity was finally designed to be ~3 μm by tilting the substrate 5° from the surface plane. ESEM and AFM images confirmed the morphology and spacing of a well-ordered holographic grating, where the periodicity was in agreement with the simulated model. In the present work, a simplified model was utilized to predict the profile of the surface holograms based

on the grating equation. More accurate simulations can be created by accounting the contribution of the refractive index and absorption of the light by the ink, and the internal reflection from the air-ink and PMMA-ink interfaces. We also demonstrated a methodology recording images with a signature and a 3D coin. Our strategy of ns laser interference recording of surface holograms is efficient and feasible to fabricate a variety of surface holograms, ranging from flat transparencies to curved or arbitrary opaque substrates (silicon-based or metallic coating). The presented approach may be applicable for printing responsive materials holograms and sensors. They also hold potential for integration with smart phone applications for the interpretation and verification of colorimetric data. These holograms are easy-to-fabricate, and low-cost, showing potential in numerous optical devices for personalized identification, security, data storage, and 3D artworks.

H.B. thanks the Leverhulme Trust for research funding. The authors thank Jeff Blyth, Christopher R. Lowe, and Yunuen Montelongo for their help toward this work.

[1]P. A. Blanche, A. Bablumian, R. Voorakaranam, C. L. W. Christenson, T. Gu, and N. Peyghambarian, "Holographic three-dimensional telepresence using large-area photorefractive polymer," Nature **468**, 80 (2010).
[2]D. E. Smalley, Q. Y. J. Smithwick, V. M. Bove, J. Barabas, and S. Jolly, "Anisotropic leaky-mode modulator for holographic video displays," Nature **498**, 313 (2013).
[3]M. Yamaji, H. Kawashima, J. I. Suzuki, and S. Tanaka, "Three dimensional micromachining inside a transparent material by single pulse femtosecond laser through a hologram," Appl. Phys. Lett. **93**, 041116 (2008).
[4]D. Xia, Z. Ku, S. C. Lee, and S. R. J. Brueck, "Nanostructures and functional materials fabricated by interferometric lithography," Adv. Mater. **23**, 147 (2010).
[5]F. D. C. Vasconcellos, A. K. Yetisen, Y. Montelongo, H. Butt, A. Grigore, C. A. Davidson, and C. R. Lowe, "Printable surface holograms via laser ablation," ACS Photonics **1**, 489 (2014).
[6]T. Kondo, S. Matsuo, S. Juodkazis, V. Mizeikis, and H. Misawa, "Multiphoton fabrication of periodic structures by multibeam interference of femtosecond pulses," Appl. Phys. Lett. **82**, 2758 (2003).
[7]W. Chen, D. C. Abeysinghe, R. L. Nelson, and Q. Zhan, "Plasmonic lens made of multiple concentric metallic rings under radially polarized illumination," Nano Lett. **9**, 4320 (2009).
[8]Z. Liu, Q. Wei, and X. Zhang, "Surface plasmon interference nanolithography," Nano Lett. **5**, 957 (2005).
[9]M. Huang, F. Zhao, and Y. Cheng, "Origin of laser-induced near-subwavelength ripples: interference between surface plasmons and incident laser," ACS Nano **3**, 4062 (2009).
[10]H. Butt, Y. Montelongo, T. Butler, R. Rajesekharan, Q. Dai, S. G. Shiva-Reddy, and G. A. Amaratunga, "Carbon nanotube based high resolution holograms," Adv. Mater. **24**, OP331 (2012).
[11]S. H. Lee, B. Cho, S. Yoon, H. Jeong, S. Jon, G. Y. Jung, and W. B. Kim, "Printing of sub-100-nm metal nanodot arrays by carbon nanopost stamps," ACS Nano **5**, 5543 (2011).
[12]J. H. Huang, Z. Y. Ho, T. H. Kuo, D. Kekuda, C. W. Chu, and K. C. Ho, "Fabrication of multilayer organic solar cells through a stamping technique," J. Mater. Chem. **19**, 4077 (2009).
[13]S. H. Lee, G. Jo, W. Park, S. Lee, Y. S. Kim, B. K. Cho, and W. B. Kim, "Diameter-engineered SnO_2 nanowires over contact-printed gold nanodots using size-controlled carbon nanopost array stamps," ACS Nano **4**, 1829 (2010).
[14]Y. Huang, J. Wu, and S. Yang, "Direct fabricating patterns using stamping transfer process with PDMS mold of hydrophobic nanostructures on surface of micro-cavity," Microelectron. Eng. **88**, 849 (2011).
[15]N. D. Lai, W. P. Liang, J. H. Lin, C. C. Hsu, and C. H. Lin, "Fabrication of two- and three-dimensional periodic structures by multi-exposure of two-beam interference technique," Opt. Express **13**, 9605 (2005).
[16]M. J. Verheijen, "E-beam lithography for digital holograms," J. Mod. Opt. **40**, 711 (1993).
[17]S. Streit-Nierobisch, D. Stickler, C. Gutt, L. M. Stadler, H. Stillrich, C. Menk, and G. Grübel, "Magnetic soft x-ray holography study of focused ion beam-patterned Co/Pt multilayers," J. Appl. Phys. **106**, 083909 (2009).
[18]A. F. Lasagni, D. F. Acevedo, C. A. Barbero, and F. Mücklich, "One-step production of organized surface architectures on polymeric materials by direct laser interference patterning," Adv. Eng. Mater. **9**, 99 (2007).
[19]A. Lasagni, T. Roch, M. Bieda, D. Benke, and E. Beyer, "High speed surface functionalization using direct laser interference patterning, breaking the 1 m^2/min fabrication speed with sub-μm resolution," Proc. SPIE **8968**, 89680A (2014).
[20]A. F. Lasagni, T. Roch, J. Berger, T. Kunze, V. Lang, and E. Beyer, "To use or not to use (direct laser interference patterning), that is the question," Proc. SPIE **9351**, 935115 (2015).
[21]T. Zhai, X. Zhang, Z. Pang, and F. Dou, "Direct writing of polymer lasers using interference ablation," Adv. Mater. **23**, 1860 (2011).
[22]Y. Li, K. Yamada, T. Ishizuka, W. Watanabe, K. Itoh, and Z. Zhou, "Single femtosecond pulse holography using polymethyl methacrylate," Opt. Express **10**, 1173 (2002).